Cerebral Cortex, 2026, 36, bhag101
https://doi.org/10.1093/cercor/bhag101
Published: 10 August 2026
Original Article

OXFORD

Distinct neural oscillations predict individual differences in feedback-guided cognitive flexibility

Judith Sattelberger[1,2,*], Hamed Haque[1,3], Liu Mengxing[4], Jaana Simola[5], Jaakko Matias Palva[1,6], Michael M. Halassa[4] and Satu Palva[1,3,*]

[1]Neuroscience Center, Helsinki Institute of Life Science, University of Helsinki, FI-00014 Helsinki, Finland
[2]BioMag Laboratory, HUS Medical Imaging Centre, Helsinki University Central Hospital, FI-00029 HUS Helsinki, Finland
[3]School of Psychology and Neuroscience, University of Glasgow, G12 8QB Glasgow, United Kingdom
[4]Department of Neuroscience, Tufts University School of Medicine, Boston, MA 02111, United States
[5]Faculty of Educational Sciences, University of Helsinki, FI-00140 Helsinki, Finland
[6]Department of Neuroscience and Bioengineering (NBE), Aalto University, FI-02150 Espoo, Finland
*Corresponding authors: Judith Sattelberger, Neuroscience Center, Haartmaninkatu 3 (PO 21), FI-00014 Helsinki, Finland. E-mail: judith.sattelberger@helsinki.fi; Satu Palva, Neuroscience Center, Haartmaninkatu 3 (PO 21), FI-00014 Helsinki, Finland. E-mail: satu.palva@helsinki.fi

Cognitive flexibility is the ability to keep or update contextual cognitive representations. The underlying neural mechanisms and how it is influenced by individual sensitivity to feedback are not known. We measured cognitive flexibility under uncertainty with the Wisconsin Card Sorting Test and brain activity with magnetoencephalography. Cognitive flexibility had large interindividual variability as indexed by the learning speed. Using a behavioral sequential learning model, we show that this variability in cognitive flexibility is predicted by individual sensitivity to feedback and anticipation and exploration tendencies, and we uncover their brain oscillatory signatures. Individual learning speed was predicted by suppressed alpha-beta (7–32 Hz) and increased broad-band gamma (32–143 Hz) amplitudes along with concurrent large-scale alpha (7–13 Hz) desynchronization. In contrast, we found no evidence for theta-band amplitudes enhancing performance directly, but rather an inverted relationship with rule certainty across a trial series. Importantly, these oscillatory sub-processes were explained by individual levels of distinct feedback sensitivity. These results provide a novel account on neural sub-computations underlying flexible feedback-guided contextual maintenance and updating of cognitive rule representations.

Significance statement

Cognitive flexibility is the ability to keep or update cognitive representations of context and allows us to make decisions under uncertainty. The ability to learn information from external cues has a large inter-individual variability, of which neural mechanisms are largely unknown. Here, we combine for the first time behavioral measures from the Wisconsin Card Sorting Task with MEG data and apply a sequential learning model to titrate the neural subcomponents underlying performance differences. We show that individual variability in learning under uncertainty is associated with differences in sensitivity to contextual cues, revealing distinct spectral profiles for learning from positive versus negative cues. Our findings demonstrate that cognitive flexibility relies on neural oscillations which are specific to the feedback cue type.

Keywords cognitive control, oscillations, synchrony, task switching, WCST

Introduction

Cognitive flexibility is a key component of cognitive control alongside top-down attention and inhibition, enabling us to quickly adapt behavior to an unpredictable and changing environment. This executive function varies widely between individuals and over the lifetime (Rhodes 2004). At its core, cognitive flexibility allows us to make decisions under uncertainty, based on cognitive rule representations whose selection depends on feedback from the environment. For example, identifying the right key of a set of unmarked keys to open a door requires remembering (i.e. using a mental map of) which key opens which door, but because such mental maps may be uncertain, a trial-and-error approach can augment the search until the right key is identified by the opening of the door. The internal representation of which key has to be used remains uncertain until the door finally

Received: February 25, 2026. **Revised:** May 31, 2026. **Accepted:** June 16, 2026

opens. A fundamental question is how such cognitive flexibility for switching between cognitive rules (or keys) under uncertainty is achieved in the brain. The ability to adapt to changing task rules, even when they are not explicitly instructed, is called task switching and has often been studied with the Wisconsin Card Sorting Test (WCST) in humans (Berg 1948; Barcelo 2003), monkeys (Mansouri et al. 2006; Kuwabara et al. 2014) and recurrent neural networks in computational work (Liu and Wang 2024). Performance in the WCST depends on multiple components, namely global and local switching, error monitoring and reward processing (Miyake et al. 2000; Gamboz et al. 2009; Nyhus and Barceló 2009), but only one study has tried to distil the impact of those sub-processes on interindividual performance variability in the WCST using a computational model that extends the traditional error type analysis of the WCST with subject-level model parameters of feedback processing (Bishara et al. 2010).

In the brain, switching between cognitive representations such as task rules depends critically on activation of the prefrontal cortex (PFC) (Buckley et al. 2009), in line with the PFC's general role in cognitive control tasks (Robbins et al. 1996; Bissonette et al. 2013; Panikratova et al. 2020), but also on activity at posterior parietal and occipital cortices (Wang et al. 2001; Periánez et al. 2004). Research in non-human animals has further shown that the mediodorsal thalamus and its interactions with the PFC are key to enabling cognitive flexibility (Rikhye et al. 2018; Lam et al. 2025). This is especially true under task uncertainty (Zhang et al. 2025), where the informativeness of external cues depends on the uncertainty of the internal rule representation (Domenech et al. 2020; Lam et al. 2025). Accumulating evidence indicates that brain rhythms—neuronal oscillations—are fundamental for temporal coordination of neuronal processing in a variety of cognitive functions (Siegel et al. 2012; Thut et al. 2012; Voytek and Knight 2015; Vinck et al. 2023). Two decades of work leveraging electroencephalography (EEG) to study overt task switching in relation to sensory representations have revealed that local theta (θ, 3–8 Hz) band oscillations in the PFC or the midline θ activity play a pivotal role in cognitive control (Duprez et al. 2020; Muralidharan et al. 2023) including conflict monitoring (Riddle et al. 2020; Sauseng and Liesefeld 2020) and anticipation (Cooper et al. 2015; Khan et al. 2025). Importantly, θ oscillations implement cognitive control also in visual working memory (VWM) (Berger and Sauseng 2022; Ratcliffe et al. 2022), speaking for their general algorithmic role in implementing frontal control functions. Local field potential data from non-human primates further show that rhythmic θ-band activity in the anterior cingulate cortex (ACC) gives rise to prominent θ-oscillations during stimulus–response mapping (Colom et al. 1988; Talk et al. 2004; Wang et al. 2005; Womelsdorf et al. 2010). In summary, θ oscillations originating in the PFC as well as ACC have been shown across various tasks depending on feedback-guided cognitive flexibility.

In addition to the ubiquitous θ-band oscillations, there is EEG-backed evidence for the role of local gamma (γ, 30–90 Hz) (Proskovec et al. 2019), parietal alpha (α, 8–12 Hz) (Verstraeten and Cluydts 2002; Foxe et al. 2014), and beta band (β, 13–30 Hz) (Gladwin et al. 2006; Cunillera et al. 2012) amplitudes in task-switching although this evidence is less consistent. Again, in VWM research, local modulation of α oscillations has been established to support top-down or feed-back attentional selection (Palva et al. 2010; Siebenhühner et al. 2016; Mamashli et al. 2021; Sattelberger et al. 2024), whereas in contrast, γ oscillations and γ-range broad band power reflect bottom-up processing and broad band increases in neuronal firing rates, respectively (Yang et al. 2021), carrying out complementary functions (Roberts et al. 2026). Crucially, the cross-frequency coupling of θ/α band oscillations with oscillations in higher β/γ frequencies via phase-amplitude coupling (PAC) enables the integration of top-down and bottom-up functions such that neurons coding for item-related information preferentially fire during particular θ phases (Ratcliffe et al. 2022) and that stimulus-related γ activity (>30 Hz) is locked to specific θ phases (Bahramisharif et al. 2018; Siegel et al. 2012). θ-γ PAC is therefore well-suited to serve as an integratory mechanism of slow and fast cognitive subprocesses. Accordingly, θ-γ PAC predicts performance variability in VWM (Axmacher et al. 2010; Biel et al. 2021; Bahramisharif et al. 2018; Brooks et al. 2020; Lisman and Jensen 2013; Peylo et al. 2022; Siebenhühner et al. 2016), attention (Cansler et al. 2023; Esghaei et al. 2022; Papaioannou et al. 2022) and feedback-processing (Chen et al. 2022; Cohen et al. 2009), but its role in cognitive flexibility under uncertainty has been remained largely unexplored.

Recent evidence, importantly, suggests that low-frequency brain oscillations could facilitate switching between the mental states associated with behavioral stability and flexibility in cognition (Ericson et al. 2025; Elmers et al. 2026). In parallel, switching between conscious sensory representations has been associated with anterior–posterior network communication and anterior information differentiation (Canales-Johnson et al. 2023). Together, these findings suggest that low frequency θ and α oscillations might provide complementary mechanisms for cognitive flexibility enabling task-switching under uncertainty. However, it has remained unknown whether the putative complementary roles of brain oscillatory activity in different frequency bands might explain the inter-individual variability in cognitive flexibility performance and uncertainty of the decision control process.

Importantly, cognitive flexibility and decision making under uncertainty is dependent on the efficient routing of information across the PFC-parietal-ACC decision circuit with sensory-motor regions (Pesaran et al. 2008; Womelsdorf et al. 2010). Such coordination is thought to be reflected in inter-areal oscillatory synchronization that could either coordinate processing via communication-through-coherence (CTC) which holds that effective communication reflects the propensity of pre-synaptic inputs to arrive at excitable phases of a receiver's oscillation (Fries 2015; Voloh and Womelsdorf 2016) or via communication-through-resonance (CTR) which holds that the energy spectrum of a neural sending population alone changes its relative impact on downstream targets depending on their resonance function (Hahn et al. 2014; Vinck et al. 2023). Inter-areal synchronization could also reflect the consequence of communication emerging from post-synaptic potentials (Schneider et al. 2021). Synchronization has been found to reflect top-down attentional selection (D'Andrea et al. 2019; Lobier et al. 2018;) and explain individual performance variability in VWM performance (Haque et al. 2025; Mamashli et al. 2021; Palva et al. 2010; Sattelberger et al. 2024; Siebenhühner et al. 2016) and multi-item attention (Rouhinen et al. 2020). Yet, no studies in humans so far have established whether inter-areal synchronization is a mechanism that supports cognitive flexibility by enabling communication of PFC and ACC with other regions.

Here, we took advantage of the rich local field potential data from magnetoencephalography (MEG) (Baillet 2017) to study the neural adaptations taking place during the WCST with excellent temporal resolution. We investigated whether low-frequency θ and α oscillations could provide complementary mechanisms for cognitive flexibility. Crucially, by applying an individualized source reconstruction approach for every test subject, MEG enables precise anatomical

mapping of neuronal sources and their inter-areal connectivity. To explain the individual variability in cognitive flexibility, we analyzed two types of errors occurring either early or late after a rule change in the task to obtain a subject-level measure of cognitive flexibility. We then implemented a new behavioral sequential learning model with which we estimated the impact of feedback processing on cognitive flexibility. Importantly, we identified which neural signatures of cognitive flexibility and rule switching were explained by sensitivity to feedback and individual anticipation and exploration tendencies.

Materials and methods

Participants

For this study, we used an existing dataset consisting of behavioral, structural MRI, and MEG data of 26 healthy adults (mean age 33.2 (SD 10.2), age range 18–57 years, 11 females) recorded by our research group. All participants reported normal or corrected-to-normal vision, no recent history of neuropsychological or neurological illness, and physical eligibility to undergo MEG and MRI measurements. The study was approved by the Helsinki University Hospital ethical committee and was carried out according to the Declaration of Helsinki. All participants provided written informed consent before the experiment.

Based on similar analysis of interindividual differences in neuronal oscillations and their relationship with behavioral performance in an earlier study (Sattelberger et al. 2024), power analysis was performed using the G∗Power software (https://www.psychologie.hhu.de/arbeitsgruppen/allgemeine-psychologie-und-arbeitspsychologie/gpower) to determine if the sample size was sufficient. We used effect sizes for amplitude and phase synchrony correlations with hit rates from that study which averaged to $r = 0.55$ and $r = 0.56$ in relevant brain areas, respectively. Power analysis revealed a sample size of $n = 23$ subjects to yield 80% statistical power at an alpha level of 0.05. Since the behavioral model parameters highly explained subject-wise differences in NLE and HR ($R^2 = 0.92$ and $R^2 = 0.91$), similar effect sizes were expected for the relationship of model parameters with amplitudes and phase synchrony.

Experimental task

Participants completed the WCST (Fig. 1a) by Berg (1948), adapted as a computerized version by Barcelo (2003) with the Presentation software (Neurobehavioral Systems, Inc., Albany, CA, USA). In the task, the participants needed to match cards according to three rule-categories: shape (circle, star, cross, or triangle), colour (blue, yellow, red, or green), or number of items (one to four). The category by which to sort changed every fifth trial and needed to be deduced by the participant through trial and error based on feedback. Participants were not informed how often the rule would change or what the next correct sorting category would be. In each trial, a sample card (bottom row), a black fixation cross, and four target cards (top row) were shown for 2.5 s before a white background. This was followed by a 1.5 s delay, during which the participant could match the stimulus card to one of the target cards, depending on the currently active rule (same number, color, or shape). A green or red feedback cross was shown for 0.25 s after the response to indicate a correct or incorrect response, and to instruct the participant to stay with the last used rule ("stay trials") or to shift to another rule category ("shift trials"), respectively. This was followed by an inter-trial delay lasting 1.9 to 2.3 s. This delay served as a time window for rule selection, so that depending on the previous feedback, the participant would shift their internal rule representation or stay at the previously chosen rule. We used this rule-selection time window for our subsequent neural analysis.

The stimulus card was a rectangle of 7.3×5.5 deg, and the target cards were rectangles of 4.2×3.0 deg visual angle. A black fixation cross (0.65×0.48 deg) and black outlines of the stimulus and target cards were present throughout the whole trial in the center of this stimulus window. The target cards remained the same for the entire experiment. The sample card was selected randomly from 24 unambiguous cards of the original 64 WCST cards (Periánez et al. 2004), meaning that only one target card fit the current rule category. As a result, only three out of the four displayed target cards shared a feature with the stimulus card and the fourth card acted as a distractor (the two green stars for the trial shown in Fig. 1a). The rule orders were selected pseudo-randomly so that the same rule was not immediately repeated. The experiment consisted of three blocks with 150 trials each, where each block had an average duration of 15 minutes and participants could rest between blocks.

Behavioural data analysis

After removal of trials without response (4% of all trials), RTs were calculated as the duration from stimulus onset to response separately for trials following negative feedback (RT_{shift}) and those following positive feedback (RT_{stay}). Hit rates (HRs) were then calculated as the proportion of correct responses from all trials. Traditionally, errors in the WCST have been divided into different error categories, with perseverative errors being associated with less cognitive flexibility, and being scored relative to the previous rule category (Berg 1948) or relative to previous response behaviour (Heaton and Staff 1993). However, in this study we did not count perseverative errors and instead pooled all errors by their position within a rule series.

We counted incorrect responses during the first two trials of a rule series as the number of early errors (NEE) and all subsequent errors as late errors (NLE), allowing us to assess the cognitive flexibility of participants across the trial set, the rationale of which we will explain here. To ensure that there was no bias in the response tendencies, we computed HRs for every trial in a rule series separately to confirm that the mean performance during early trials was at a chance level and exceeded thereafter. We defined the chance level as follows under the presumption that the task instructions were followed correctly. Chance level at trial 1 of a new rule series should be 0% because the participants are not informed about rule changes, so that the experimental expectation is to choose the card that belongs to the previous series' rule category which is never correct. At trial 2, the participant is aware that the last chosen category does not apply anymore, leaving two possible card options (50% chance level) and one distractor card that does not share any features with the stimulus card. Hereafter, the participant has sufficient information to know the correct rule category (100% chance level) and all errors made in trials 3 to 5 can be attributed to cognitive causes (i.e. slow learning) rather than statistical uncertainty. HRs, NLE, NEE were computed across all trials for each participant. To assess response speed, we computed mean RTs across trials for Shift (RT_{shift}) and Stay (RT_{stay}) trials.

For statistical comparisons of behavioral data, we used equivalent tests of both frequentist and Bayesian statistics (JASP Team 2024). Statistical testing between the conditions (Shift vs. Stay) in RTs was performed with a two-tailed *t*-test for paired samples. To estimate the

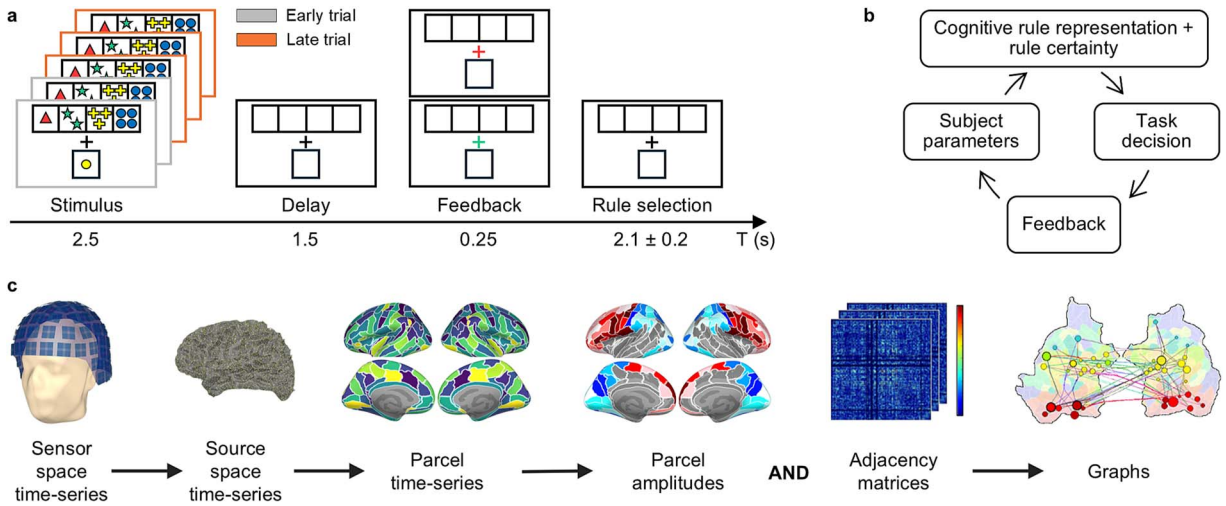

Figure 1 Experimental paradigm. a. Schematic of the Wisconsin card sorting test. In each trial, a new sample card (bottom row) and the four target cards (top row), were shown, followed by a delay during which the participants were to match the sample card to one of the target cards based on a changing rule. A colored feedback cross was shown after the response, followed by a delay that allowed for selection of a cognitive rule for the next trial. b. Schematic of the behavioral modeling. In the beginning of each trial, the participant had a cognitive rule representation, based on which they made a task decision to match the card to one of the three categories, leading to positive or negative feedback. Depending on the subject's individual tendency to respond to feedback as estimated by the subject parameters, this feedback modified the rule representation and increased the certainty of that rule. c. Schematic of the MEG analysis. Cortical sources were reconstructed from broad-band MEG time-series data, collapsed into cortical parcels and used for estimating oscillation amplitudes and phase-synchronization between parcels.

presence of a speed-accuracy trade-off, we computed the correlation of RT_{shift} and RT_{stay} with NLE across subjects using the Pearson correlation coefficient. To assess the co-variance of HR, NLE, RT_{shift}, and RT_{stay} with age we computed the Pearson correlation coefficient with these measures and we likewise used independent-samples t-tests to estimate the influence of sex. For these tests, we reported the frequentist test parameters and also the Bayes Factors (BF10) as the likelihood of the independent variables to explain our data.

The sequential learning model

To further assess the individual factors underlying behavioral performance also at the single-trial level, we developed a sequential learning model based on Bishara et al. (2010), Fig. 1b). The model tracks an attention weight vector $\alpha \in \mathbb{R}^3$, whose three elements represent the probability of the currently active rule is shape, number, or color respectively (initialized uniformly at [⅓, ⅓, ⅓]). On each trial, the probability of choosing pile *j* is:

$$P(j) = \frac{m_j \cdot \alpha}{\Sigma_k m_k \cdot \alpha}$$

where m_j is the match vector for pile j ∗1 for the dimension consistent with choosing that pile, 0 otherwise). After each trial, α is updated based on the participant's choice and the resulting feedback:

$$\alpha \leftarrow (1-\lambda)\,\alpha + \lambda s$$

where λ = r (reward sensitivity) on correct trials with s = m{chosen}, and λ = p (punishment sensitivity) on incorrect trials with s = 1—m{chosen}. The parameter *r* and *p* are taken directly from Bishara et al. (2010). Despite our task delivering only positive and negative feedback rather than monetary outcomes, we retain the original terminology. Trial-wise rule certainty was derived from the Jensen-Shannon distance between α at consecutive trials, which is largest immediately after a rule shift and decreases as feedback confirms the new rule. Rule certainty was then defined as 1 minus this distance.

To formally establish whether two additional task-specific parameters improved model fit, we compared three nested models. The baseline model M1 contains only r and p as described above. The second model M2 adds an anticipation tendency parameter a, motivated by the fixed 5-trial rule change interval in our task design, which has no analogue in the original Bishara et al. (2010) paradigm that used a variable schedule. In M2, at the start of each new rule block the dominant element of α is downweighted by a factor (1-a) and its weight redistributed equally to the other two dimensions, capturing the tendency to proactively disengage from the current rule when a change is expected. The third and final model M_{final} further adds an exploration tendency parameter e, motivated by the observation that participants occasionally chose a non-dominant pile even when rule certainty was high. This is implemented by mixing the model-derived choice probability with a uniform distribution, such that the effective probability of choosing pile j becomes (1-e)P(j) + e/4, reflecting random exploration independent of the current attention state.

Parameters were estimated for each participant by minimizing the negative log-likelihood of the observed choice sequence. Model fit was evaluated using the Bayesian Information Criterion (BIC), which penalizes model complexity (Supp. Fig. 1). M2 provided a substantially better fit than M1 (mean ΔBIC = −90.60), confirming that the anticipation of the fixed rule-change interval meaningfully improved the account of participants' behavior. M_{final} provided further improvement over M2 (mean ΔBIC = −122.55), supporting the inclusion of the exploration tendency parameter. All further analyses therefore use the parameters estimated from M_{final}.

Our analysis revealed two outlier subjects with a punishment sensitivity $\boldsymbol{p}$ below 0.1 (deviating from the mean by more than 2 SDs) due to minimal error trials, so we removed these subjects from further analysis of the model's subject parameter data. We then used multiple linear regression models to investigate if these parameters could

explain differences in NLE, HRs and RTs and reported the Bayes Factor of the model (BFM) compared to the null model as well as each parameter's Bayes Factor for model inclusion (BFi). The statistical significance of increased rule certainty across trials of a rule series was assessed with frequentist and Bayesian Analysis of Variance (ANOVAs).

MEG and MRI recordings, preprocessing and filtering

Participants sat approximately 57 cm from the screen (BenQ, height: 30 cm, width: 53 cm, resolution: 1920 × 1080, 60 Hz refresh rate). Stimuli were presented with the Presentation software (Neurobehavioral Systems, Inc., Albany, CA, USA) and a photodiode was used to achieve ±1 ms precision of stimulus presentation. We recorded MEG with 204 planar gradiometers and 102 magnetometers with a Triux (Elekta Neuromag Ltd) system at 1000 Hz sampling rate and an online bandpass filter of 0.03–330 Hz at the BioMag Laboratory in the Helsinki University Hospital. Ocular artifacts were measured with electrooculogram electrodes. Participants' responses were recorded with a hand-held fiber-optic response device that responded to finger lifts.

In addition, whole head magnetic resonance images (MRIs; Siemens Verio 1.5 T) were taken from all subjects for the source-reconstruction of MEG data with the magnetization-prepared rapid acquisition gradient echo sequence at a resolution of 1 mm voxel size. Maxfilter software (Elekta Neuromag) was used for temporal signal space separation to suppress extra-cranial noise in MEG data, to adjust for head position changes during the measurements, and to interpolate bad channels (Taulu and Kajola 2005). Head position changes over 10 mm were excluded from the raw data and raw MEG data was then notch-filtered at 50 Hz and harmonics. Independent component analysis was used for identifying and extracting ocular and heartbeat artifacts. The MEG data was then frequency-filtered using 38 approximately logarithmically spaced Morlet wavelets from 3 to 143 Hz with m = 5 cycles.

MEG source modeling

In order to obtain precise source localization of MEG signals optimized for every participant's individual brain anatomy, we applied a multistep source modeling approach (Fig. 1c). The open-access software Freesurfer (http://surfer.nmr.mgh.harvard.edu) was used for volumetric segmentation of the MRI data, surface reconstruction, flattening, and cortical parcellation/labeling with the Destrieux atlas, resulting in 200 source-localized parcels that correspond to functionally homogeneously grouped cortical areas. The software MNE-Python (https://mne.tools/stable/index.html) was used for MEG-MRI colocalization, and preparation of the forward and inverse operators. For every subject, we created the source space with dipole orientations fixed to the pial surface normals and a 5 mm inter-dipole separation, a 1-layer boundary element method (BEM) model from the inner skull, and the BEM solution. To compute noise-covariance matrices (NCMs), we used a regularization constant of 0.05 and narrowband 151–299 Hz filtered resting-state data (1 min), which we recorded from each participant prior to the WCST in the same session. NCMs were then used to compute a forward solution and the inverse operator that transform the filtered complex single-trial MEG time series to source-vertex time series. Source-space vertices were collapsed into 400 cortical parcels using fidelity optimized collapse operators (Korhonen et al. 2014), assigning each parcel to one of 7 functional networks before morphing them into 200 larger parcels to increase statistical power.

Data analysis

The time window of rule selection was used for all neural analysis. To extract this time window and an appropriately long baseline from the time series, we used 2.5 s epochs spanning from 0.55 s prior to feedback onset to 1.95 s after. Trials with clear artifacts during the baseline such as blinking were removed to avoid contamination during baseline correction. Single-subject oscillation amplitudes were computed for each wavelet frequency and for each parcel as an average across all trials of each condition (Shift and Stay), from which the baseline (0.5–0 s prior S1 onset) was then subtracted. Single-trial amplitudes were computed for the analysis of the trial order effect using the same approach but not averaging across the trials. To increase statistical power for condition-averaged and single-trial amplitude data, we averaged amplitudes within smaller time windows of 100 ms length that overlapped by 50 ms.

Phase-synchronization was computed for each wavelet frequency and between all parcels separately for both conditions and each subject. We first excluded 3 subjects with a small number of shift trials ($n < 60$) that did not yield sufficient effect sizes for the estimation of phase synchronization and equalized the number of trials between conditions to the lowest number within each subject as oscillation phase measures are sensitive to the number of trials. We then averaged the complex signal across trials for each condition and subject in smaller time windows of 400 ms length and 300 ms overlap, and computed the imaginary part of the phase locking value (iPLV) between each parcel-parcel pair for every time window. Single-trial phase synchronization was not estimated due to insufficient data points resulting from the file saving format. These data were baseline-corrected by subtracting the mean iPLV of the first time window (0.4–0 s prior S1 onset).

While using iPLV to estimate inter-areal synchronization excludes the direct effects of zero-phase lagged signal mixing, spurious interactions still remain (Palva et al. 2018). We therefore removed edges (pairwise connections) between parcels for which the source reconstruction accuracy, fidelity, was below 0.1 (3.5% of parcels). To further exclude spurious connections, we removed edges between parcels that exhibited the greatest signal leakage with their neighbors, measured with cross-patch PLV (fidelity radius greater than 0.4). A total of 17.8% of all possible edges were thus excluded from the analyses. This created adjacency matrices for each frequency and for each subject that defined a graph made up of nodes and edges, where nodes are cortical parcels and edges are the connections between nodes.

To then estimate n:m PAC, we compared the phase of all low frequencies (3–8 Hz) to the phase of the amplitude envelope of high frequencies (9–143 Hz) by computing the PLV between all edge pairs. This was done for each subject and for the averaged trials of conditions Shift and Stay separately, in the time window 0.6 to 1.6 s after feedback onset. Because PLV is sensitive to the number of trials, we equalized the number of trials between conditions to the lowest number within each subject before averaging, again excluding the three subjects with $n < 60$ Shift trials.

Statistical analysis of neuronal data

Group-level statistical analyses of neuronal effects were then carried out. For oscillation amplitudes, statistical analyses were carried out separately for each parcel, time window and frequency across subjects. For inter-areal phase-synchronization and PAC, the statistical

analysis was carried out per each edge (parcel-parcel connection), time window (only one for PAC) and frequency across subjects.

A two-sided Wilcoxon-signed rank test at $\alpha = 0.05$ was used for testing statistical differences between either condition (Shift and Stay) and the baseline, as well as their contrast, Shift-Stay. To estimate statistically significant correlations of oscillation amplitudes, inter-areal synchronization, and PAC with NLE, RT_{shift}, and RT_{stay}, we calculated Spearman's r at $\alpha = 0.05$ for every frequency, time window and parcel or edge. To estimate the effect of trial series on single-trial amplitudes, Spearman's r at $\alpha = 0.05$ was also used to compute statistically significant changes in oscillation amplitudes across a trial series for every frequency, time window and parcel. We furthermore calculated Spearman's r at $\alpha = 0.05$ to assess the correlation of the model subject parameters with the condition-averaged amplitude and phase synchronization across subjects, separately for every frequency, time window and parcel or edge.

To estimate the robustness of oscillation amplitude modulations and that of changes in inter-areal phase synchronization across the whole cortex, we calculated the fraction of cortical parcels with a significant effect out of all 200 parcels (P) and similarly, the connection density (K), which is the fraction of significant edges out of all 39,800 edges. For phase synchrony, statistical thresholding was further used to construct two group-level adjacency matrices that contained the average iPLV of significant edges across time and frequencies where the non-significant values were set to zero, for the θ- and α-band.

When analysing statistical significance of oscillation amplitude and phase synchrony effects, we then removed false positives caused by multiple statistical tests by pooling all significant observations over all parcels for amplitude analysis and edges for synchrony and then discarded a percentage of the least-significant comparisons predicted to be false discoveries equivalent to the α level (Palva et al. 2010; Siebenhühner et al. 2020). To remove any remaining false positives, a threshold q was defined for the number of significant observations that could arise by chance in any of the frequencies even after controlling for multiple comparisons (Puoliväli et al. 2020). This was estimated by simulating random processes at the null hypothesis, using the same number of tests performed in the actual experiment, and recording the residual fractions of significant observations after the elimination of the number of significant observations predicted to be false positives by the α level. Given the number of cortical parcels and time windows in which statistical analyses were performed for each condition, q was estimated to correspond to 8% of parcels and 0.67% edge density and was removed from the fraction of significant parcels (P) or the connection density (K). We only visualized oscillation amplitude modulations and inter-areal synchronization changes that exceeded the q threshold across frequencies in time-frequency representations (TFRs).

For statistical analysis of PAC at the group level, we estimated the statistical significance of each pairwise interaction for each of the 1:m ratios. We identified interactions that were significantly stronger or weaker in the Shift and Stay conditions than at baseline by computing time-shifted surrogate data and deeming connections with a ratio of 2.42 (corresponding to $P < 0.01$) or higher as significant. Spurious connections were removed by estimating amplitude coupling between low and high frequencies and identifying triangle motifs (Siebenhühner et al. 2020), after which we removed edges below the q threshold of 3.5% as described above. Shift- and Stay-condition PAC were contrasted using a two-sided Wilcoxon signed-rank test with a statistical significance level $P < 0.05$ and corrected for multiple comparisons by removing the 5% largest p-values as well as edges below the q threshold of 0.39%. The trial order effect and behavioral correlations were again corrected for any remaining false positives by applying the thresholding with q = 0.28%.

Post-hoc analyses were carried out on time-frequency (TF) windows of interest that were selected to contain the most robust (largest P values for amplitude and K for phase synchronization) significant neuronal effects. This includes the estimation of effect sizes, for which we calculated the average difference between all parcels/edges within the described TF windows of interest as $r = Z/\sqrt{N}$ (Rosenthal 1991). We also obtained the mean graph strength (mean GS) of the averaged edges within functional networks in the TF windows of interest of the θ- and α-band from the thresholded adjacency matrix.

Finally, we investigated whether amplitude modulations in the θ-band (3–6 Hz) or α-band (9–13 Hz), in which significant effects in amplitude and phase synchrony overlapped, could explain similar modulations of phase synchronization, i.e. if changes in iPLV in the respective frequency bands were reducible to differences in phase estimation reliability due to changes in the signal-to-noise ratio. To this end, we estimated the correlation between θ and α-band amplitude and iPLV network strength across participants in the rule selection window, both for averaged conditions and only for the Shift-Stay contrast (Lobier et al. 2018; Sattelberger et al. 2024). Unreliable parcels as outlined above were removed before estimation of mean subject oscillation amplitudes and graph strength. For each subject, mean graph strength (GS) was then computed as the average iPLV of all remaining edges and mean amplitude was calculated as the average of all remaining parcels. Correlations were thus computed across the 193 parcels having at least one possible edge using Spearman's r.

Graph visualization

The spectro-temporal patterns of phase synchrony and PAC modulations were first visualized as TFRs, in which we identified the frequency bands and TF windows with the most robust effects. We then showed the most important hubs and connections in those networks as graphs by visualizing the edges that were significant in more than 15% of the TF bins across the selected time and frequencies of the thresholded adjacency matrix.

Node centrality metrics were further used to identify highly connected nodes in the graphs that putatively play a key role in network communication. Here, we used the graph metric *Degree,* that is the number of edges of a node to other nodes, to select the most connected nodes which act as communication hubs in the network. We then visualized graphs that contained the nodes that were within the 65th percentile of largest-degrees and their 200 strongest edges, i.e. the edges with the highest iPLV for phase synchrony and PLV for PAC. To further mitigate the contribution of spurious interactions caused by the concurrent presence of true interactions and linear mixing, a hyperedge-bundling approach was used in the visualization (Wang et al. 2018). The hyper-edges thus bundled together edges that putatively originated from a single true edge among the spurious edges caused by source-leakage (Palva et al. 2018).

Results

In this study, 26 healthy participants completed a computer-based version of the WCST in which the active sorting rule (out of three possible rules) changed after every fifth trial (Fig. 1a). This task thus

allows the separation into conditions with maintenance (Stay trials, in which the participant is instructed to repeat the previous rule) and updating (Shift trials, where the internal rule needs to be changed) of cognitive representations, so that the subject's performance across the trial set measures cognitive flexibility. As the subjects were not informed about the rule change interval, the active rule needed to be sorted out from negative (Shift) or positive feedback (Stay), which we analyzed with a sequential learning model (Fig. 1b). With this model, we estimated the currently active cognitive rule representations and, based on the presence or absence of behavioral switches between categories within a trial set, the trial-to-trial rule certainty. By combining the subject's task decisions and feedback across trial sets, we obtained the subject parameters of positive and negative feedback processing. MEG data during rule selection were source-reconstructed using individual anatomical MRIs and collapsed into a cortical parcellation of the Schaefer atlas and filtered with Morlet wavelets between 3–143 Hz. A data-driven approach was then used to compute local and inter-areal oscillation dynamics for all frequencies and for all parcels or parcel-pairs, respectively (Fig. 1c).

Behavioral performance

In the WCST task, the participants needed to match cards according to three rule-categories: shape (circle, star, cross, or triangle), color (blue, yellow, red, or green), or number of items (one to four). The category by which to match changed on every fifth trial unknown to the participants, so that the rule needed to be deduced based on feedback on whether the preceding selected rule was correct (green cross) or incorrect (red cross). Consequently, if the selected rule was correct, the participant could "stay" at the current rule during the next trial, while if it was incorrect they were to "shift" to a different rule. This allowed us to measure the neural signatures of maintaining (Stay trials) vs. updating (Shift trials) cognitive rule representations across participants and further, to investigate how individual differences in the ability to switch between representations depended on the participants' sensitivity to feedback. To characterize the variability in the accuracy and rapidness of switching between representations, we categorized incorrect responses during the first two trials of a rule series as early errors (EE) and all subsequent errors as late errors (LE). The rationale for this division was that from the 3rd trial onwards, the participant had sufficient information to know the correct rule category (1 card never matched plus 2 previous feedbacks had been given) and all errors made thereafter could be attributed to cognitive mistakes rather than statistical uncertainty. Calculating the number of late errors (NLE) allowed us thus to assess the participant's errors in cognitive switching beyond chance rate. Across participants, there was a high variability in NEE and NLE, establishing that there are large individual differences in cognitive flexibility, i.e. the tendency to maintain the current or switch to new cognitive representations under uncertainty (Fig. 2a).

However, generally, participants' higher number of EE (NEE; M = 119.3, SD = 27.8) than NLE (M = 47.9, SD = 38.9) reflected their rule learning across a rule set of five trials. This was further visible in HRs increasing with every trial within a rule set, showing a clear gradient in HRs from early to late trials (Fig. 2b). Importantly, participants were not able to learn the rule change interval of 5 trials with the majority of subjects' HRs at early trials still being low (median = 0.07, mean = 0.20, SD = 0.27), except for three subjects with the highest anticipation tendency ***a***. These participants also had the highest HRs in block 3, marking them as the highest performers in our experiment (Supp. Fig. 2).

RTs were on average 102 ms longer in shift than stay trials (Fig. 2c; $T(25) = 6.01$, $P = 2.81e\text{-}6$; BF10 = 6879.316), meaning that participants reacted more slowly after having received negative feedback. Additionally, both RT_{shift} (r = 0.52, $P = 0.0065$, BF10 = 8.110) and RT_{stay} (r = 0.52, $P = 0.0063$, BF10 = 8.398), but not their difference RT_{shift}—RT_{stay} (r = 0.05, $P = 0.7963$, BF10 = 0.251), were positively correlated with NLE across participants (Fig. 2d). Differences in behavior were neither confounded by age [HR (r = −0.13, $P = 0.514$, BF10 = 0.298), NLE (r = 0.05, $P = 0.827$, BF10 = 0.249), RT_{shift} (r = 0.11, $P = 0.573$, BF10 = 0.283), RT_{stay} (r = 0.16, $P = 0.422$, BF10 = 0.331)] nor sex [HR ($T(24) = -1.281$, $P = 0.212$, BF10 = 0.664), NLE ($T(24) = 1.220$, $P = 0.234$, BF10 = 0.629), RT_{shift} ($T(24) = 1.159$, $P = 0.258$, BF10 = 0.597), RT_{stay} ($T(24) = 1.382$, $P = 0.180$, BF10 = 0.730)].

With our behavioral model, we first estimated the trial-to-trial rule certainty by creating an attention-weight-vector that represents the participant's chosen rule in the previous trial (Bishara et al. 2010), whereby the rule certainty is calculated as the inverted Jensen-Shannon distance between weight vectors. This allowed us to investigate trial-to-trial changes associated with the participant's certainty of the rule representation across a series of trials within a given rule set (Fig. 2e), which overall increased with every trial of a rule series from a mean value of 0.242 at the first trial to 0.913 at the fifth trial ($F(4) = 297.209$, $P < .001$, BF10 = 8.226e+55). To then investigate how cognitive flexibility was driven by differences in the sensitivity to positive (reward) or negative (punishment) feedback at the single-trial level for each individual, we implemented a sequential learning model with which we estimated the subject-wise parameters for reward sensitivity ***r*** and punishment sensitivity ***p*** measuring error monitoring as in Bishara et al. (2010). In addition, as new behavioral measures, we estimated the exploration tendency ***e*** and anticipation tendency ***a*** which assessed the effect of rule shifting despite preceding positive feedback and the subjects' ability to predict an upcoming rule change after 5 trials, respectively (Fig. 2f). We then used multiple linear regressions to reveal the explanatory value of these parameters on HRs, RTs and NLE. The model was significant for HRs ($F(4,21) = 62.703$, $P < .001$, $R^2 = 0.923$, BFM = 3.852) and NLE ($F(4,21) = 70.818$, $P < .001$, $R^2 = 0.931$, BFM = 29.342), but not RT_{stay} ($F(4,21) = 1.619$, $P = 0.207$, $R^2 = 0.236$, BFM = 0.500) or RT_{shift} ($F(4,21) = 1.593$, $P = 0.213$, $R^2 = 0.233$, BFM = 0.499), establishing that the accuracy but not response times depend on individual feedback sensitivity. The regression equation for HR was thus $HR = 0.277 + (0.141\boldsymbol{r}) + (0.315\boldsymbol{p}) - (0.361\boldsymbol{e}) + (0.430\boldsymbol{a})$ where all parameters but ***r*** were significant (***r***: $P = 0.108$, BFi = 1.212; ***e***: $P = 0.017$, BFi = 9358.513; ***a:*** $P < 0.001$, BFi = 3.205; ***p***: $P < 0.001$, BFi = 2.909e+06). The number of late errors were explained by $NLE = 153.2 - (62.5\boldsymbol{r}) - (97.5\boldsymbol{p}) + (191.8\boldsymbol{e}) - (62.9\boldsymbol{a})$ with all parameters significant (***r***: $P = 0.018$, BFi = 7.478; ***p***: $P < 0.001$, BFi = 9733.338; ***e***: $P < 0.001$, BFi = 231.102; ***a***: $P < 0.001$, BFi = 589.644).

Responsivity to positive and negative feedback positively covaried across subjects (Pearson's r = 0.41, $P = 0.047$, BF10 = 1.634), so that participants with a higher reward sensitivity tended also to be more sensitive to punishment. Reward sensitivity predicted NLEs weakly while the punishment sensitivity was a strong predictor of NLE across subjects (Fig. 2g; ***r***: Pearson's r = −0.46, $P = 0.023$, BF10 = 2.865; ***p***: Pearson's r = −0.75, $P < 0.001$, BF10 = 1028.328), demonstrating the distinct effect of positive and negative feedback on improvements in the behavioral outcome. Additionally, participants with a larger exploration tendency had a higher NLE (Fig. 2h; ***e***: Pearson's r = 0.62,

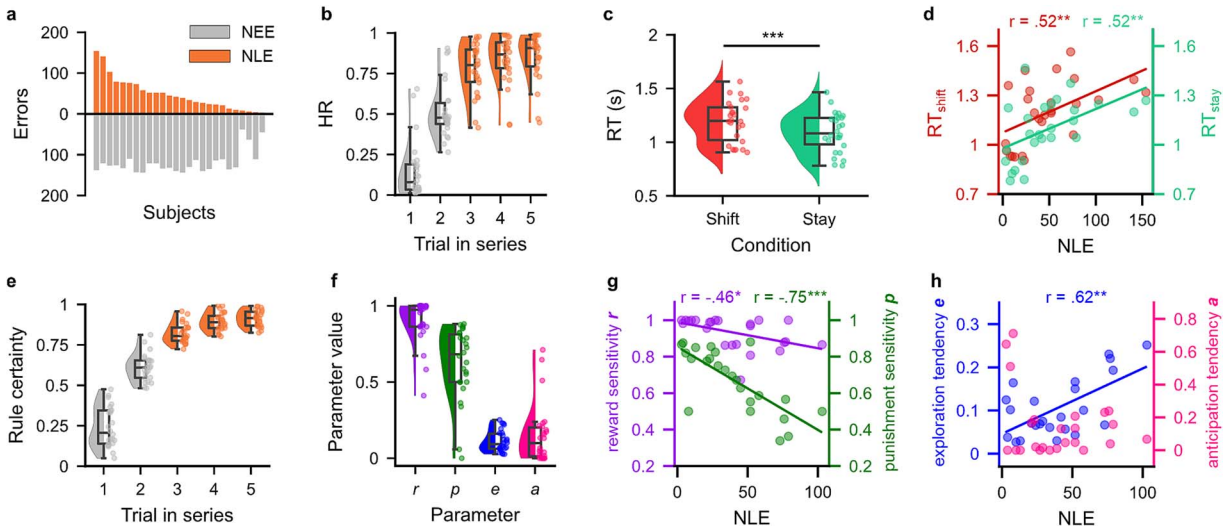

Figure 2 Behavioral results and results of the sequential learning model. a-d. Behavioral outcomes. a. Number of early and late errors (NEE and NLE) by subjects ($n = 26$). b. Averaged HRs for every trial in a rule set. The half violin plots and boxplots show the distribution and median values of HRs, and the dots the subjects' means. c. the difference in RTs for shift and stay conditions between subjects. Asterisks indicate significant differences (Wilcoxon signed-rank test, $^{*}P < 0.05$, $^{**}P < 0.01$, $^{***}P < 0.001$). d. Scatterplot of the correlations of RTs with NLE across participants. Colored fitting lines indicate the significant correlation of NLE with RT_{shift} (red, left y-axis) and RT_{stay} (green, right y-axis). Asterisks indicate a significant correlation (Pearson's r). e-h. results of the behavioral model. e. Mean rule certainty by trial order and across subjects. f. Parameter values across subjects. g and h. Correlations of all subject parameters with NLE across participants after outlier exclusion ($n = 24$). Dots represent each subject's value in reward sensitivity (purple, left y-axis), punishment sensitivity (green, right y-axis), exploration tendency (blue, left y-axis) and anticipation tendency (pink, right y-axis), and colored fitting lines indicate significant correlations of the respective subject parameter with NLE.

$P = 0.001$, BF10 = 35.356), whereas the tendency to anticipate upcoming rule changes did not significantly impact learning speed ($\boldsymbol{\alpha}$: Pearson's r = −0.28, $P = 0.185$, BFi = 0.581).

Oscillation amplitudes predict individual differences in feedback processing

To investigate the neural mechanism underlying these behavioral effects, we computed oscillation amplitudes from individually source-reconstructed MEG data (Fig. 1c). We first computed these for the Shift and Stay trials focusing analysis on the rule selection period, during which participants decided whether to maintain the current cognitive representation for the rule or update it for a new rule. We compared Shift and Stay trials to the pre-stimulus baseline (Supp. Fig. 3a) and then calculated significant differences between the two conditions (Fig. 3a, Wilcoxon signed-rank test, $P < 0.05$, q = 0.08). Shift trials were characterized by stronger sustained theta-band (θ, 3–6 Hz) oscillations and a concurrent suppression of alpha (α, 7–13 Hz) and beta (β, 13–32 Hz) band oscillation amplitudes than the Stay condition throughout the rule selection period. In addition, the Shift condition was also associated with an increase in broad-band gamma (γ, 42–143 Hz) amplitudes that were absent in the Stay condition. These amplitude modulations had medium to strong effect sizes (Supp. Fig. 3b, θ: $P = 2.03e\text{-}34$, r = 0.87; α: $P = 6.88e\text{-}16$, r = 0.57; β: $P = 3.28e\text{-}26$, r = 0.75; γ: $P = 9.65e\text{-}31$, r = 0.82). Differences in θ-band oscillation amplitudes were widespread across frontal, temporal and visual cortices, whereas α and β amplitudes were suppressed over parietal areas with a concurrent amplitude increase in the left lateral (sub-)orbital sulcus and the bilateral primary visual areas, largely overlapping between the two frequency bands (Supp. Fig. 3c). Increases in γ amplitudes were located in the left cingulate cortices, precuneus, insula and orbitofrontal cortex and the parcels of V1 (right calcarine sulcus and cuneus).

Next, to study whether oscillation amplitude modulations would change as participants learned the currently active rule, we computed the correlation of oscillation amplitudes with trial order, i.e. the position of the trial within a rule set (Fig. 3b, Spearman's r, $P < 0.05$, q = 0.08). Participants showed smaller θ amplitudes between 0.9–1.8 s after feedback, and increased $\alpha - \beta$ amplitudes (0.5–1.35 s after feedback) as the rule set progressed, indicating that the $\theta - \beta$ amplitudes underwent a spectral transition from rule shifting towards staying at the correct rule. To further understand the neural basis of individual variability in behavioral measures of cognitive flexibility, we investigated how the condition-averaged amplitudes would predict differences across individuals in accuracy and RTs. Individual variability in switching behavior, especially variability in NLE, but also in RT_{shift} and RT_{stay}, correlated positively only with $\alpha - \beta$ (7–24 Hz) and γ (32–143 Hz) amplitudes while there was no effect in the θ amplitude (Fig. 3c).

Positive correlations of $\alpha - \beta$ band amplitudes with NLE overlapped largely, leading us to combine the two, and were found in the striate cortices, posterior parietal cortex (PPC), and in the medial PFC including insular and suborbital cortices (Fig. 3d). In addition, NLE was correlated negatively with broad-band γ amplitudes arising from the parcels in the visual system, the intraparietal sulcus (IPS) of the PPC, and from both the lateral and medial PFC including anterior cingulate cortices. Thus, participants with fewer NLE had smaller $\alpha - \beta$ amplitudes over the PPC and larger γ-band activity, reaching a mean correlation strength of r = 0.55.

We next used the model parameters to distill the oscillatory subcomponents underlying cognitive flexibility We first used trial-to-trial rule certainty as a regressor for oscillation amplitudes to understand the effect of rule representation stability on local neural activity. Higher rule certainty was associated with smaller θ band and larger $\alpha - \beta$ band amplitudes (Fig. 3e) similarly to the trial order correlation indicating that the spectral amplitude transition across a trial series

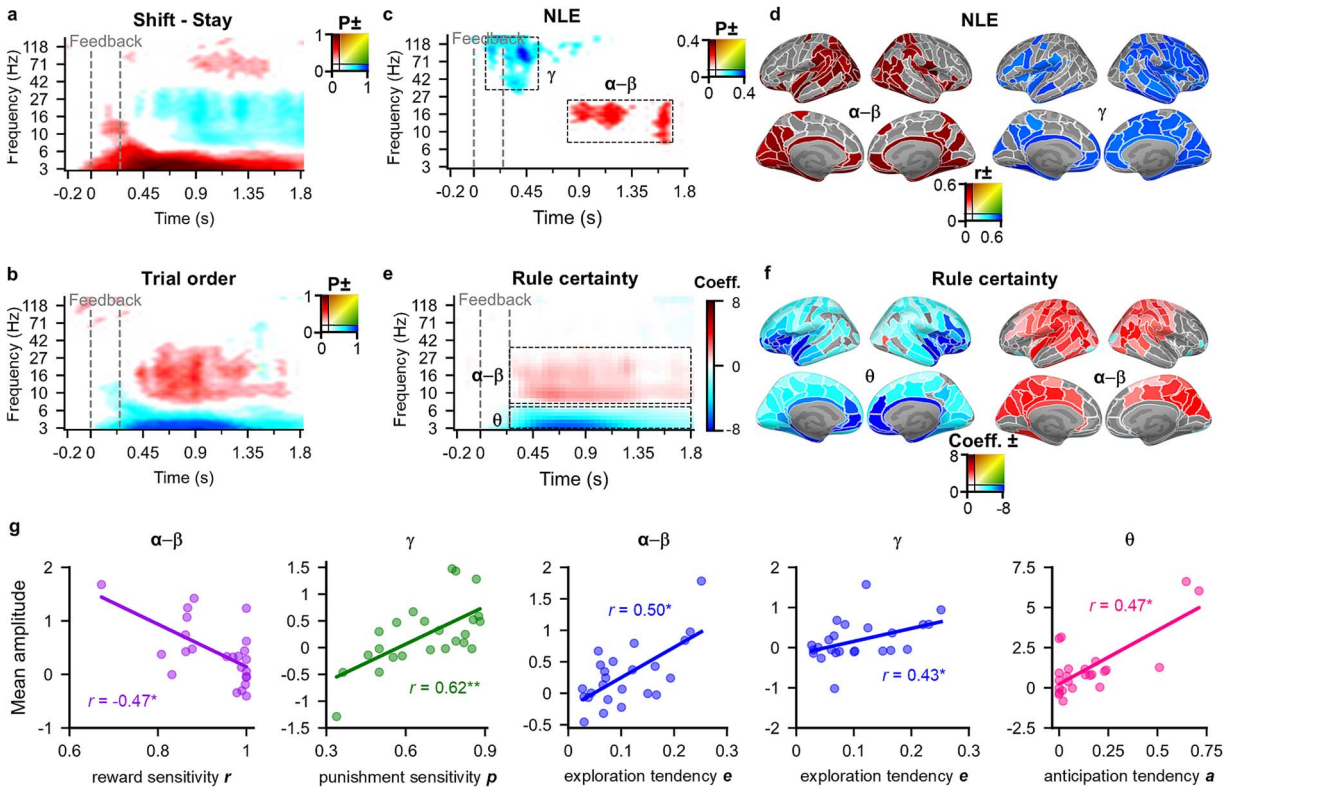

Figure 3 Oscillation amplitude effects. a. Group-averaged oscillations amplitudes for the shift and stay trials compared to the baseline, and their contrast ($n = 26$). Color indicates the fraction of parcels (brain regions) (P) with a statistically significant effect (Wilcoxon signed-rank test, $P < 0.05$, FDR corrected, q = 0.08). The dashed black box indicates the time-frequency (TF) bins of interest during rule selection. b. the fraction of parcels whose amplitude significantly increased or decreased across a rule set (Spearman's r, $P < 0.05$, FDR corrected, q = 0.08). c. Correlation of parcel amplitudes with NLE, and the shift and stay RTs (Spearman's r, $P < 0.05$, FDR corrected, q = 0.08). d. Oscillation amplitudes explained by increasing rule certainty within a trial series, where colors indicate the coefficients of parcels with a significant model fit (linear regression, $P < 0.05$, FDR corrected, q = 0.08). e. Brain parcels with a significant correlation with NLE. Color indicates the correlation coefficients. f. Brain parcels with a significant increase in rule certainty across trials. Color indicates the regression coefficients. g. Relationship of mean amplitudes of shift and stay trials over all parcels with a significant model fit and the subject parameters. One circle represents one subject, and lines indicate the fit across subjects ($n = 24$).

was related to increased rule certainty. The spectral changes associated with increasing rule certainty were most prominently seen in the PFC in the θ band and over the PPC in the $\alpha - \beta$ band (Fig. 3f).

We then investigated how subject-wise differences in feedback sensitivity predicted variability in oscillation amplitudes (Supp. Fig. 4a). The $\alpha - \beta$ band amplitude suppression related to rule switching and rule certainty was best explained by the reward sensitivity $\boldsymbol{r}$ so that subjects who were more sensitive to positive feedback showed more decreased $\alpha - \beta$ amplitudes ($P = 0.018$) (Fig. 3g). In contrast, anticipation tendency $\boldsymbol{a}$ was predicted by a sustained θ (3–8 Hz, 1–1.8 s) amplitude increase ($P = 0.019$).

In addition, the sustained broad-band γ-response differentiating Shift-Stay trials correlated positively with the punishment sensitivity $\boldsymbol{p}$ and exploration tendency $\boldsymbol{e}$ (43–143 Hz, 0.5–1.8 s) ($\boldsymbol{p}$: $P = 0.0012$, $\boldsymbol{e}$: $P = 0.036$). Furthermore, exploration tendency $\boldsymbol{e}$ also predicted a transient increase in $\alpha - \beta$ amplitudes ($P = 0.013$). These feedback-specific neural processes displayed distinct anatomical distributions across the cortex, however mirroring the effect localizations of Shift-Stay amplitude differences in the respective frequency bands (Supp. Fig. 4b). Hence, we found specific neural oscillatory subprocesses to underlie covert task switching under rule uncertainty and to reflect differences in feedback processing.

α desynchronization predicts individual behavioral cognitive flexibility

To resolve whether oscillation-based functional connectivity could reflect cross-cortical routing of information processing to enable cognitive flexibility, we computed inter-areal phase synchronization that indicates the statistical temporal regularities between brain areas. To this end, we computed inter-areal phase synchronization with the imaginary phase-locking value (iPLV) between all cortical parcels and for all frequencies, separately for Shift and Stay trials against the baseline (Supp. Fig. 5a) and then the difference between the two conditions (Fig. 4a, Wilcoxon signed-rank test, $P < 0.05$, q = 0.0067). Both the Shift and Stay conditions were characterized by strong θ-band synchronization that was sustained throughout the rule selection period and by a later onset α-band desynchronization, both of which were stronger for the Shift than Stay condition. However, trial order was only correlated with a decrease in θ band synchronization (Fig. 4b), indicating that the synchronization decreased as the rule set progressed from Shift towards Stay trials and i.e. that synchronization was specifically related to instructed updating of the internal rule representation. The largest differences between Shift and Stay conditions had a medium effect size in the θ band (Supp. Fig. 5b,

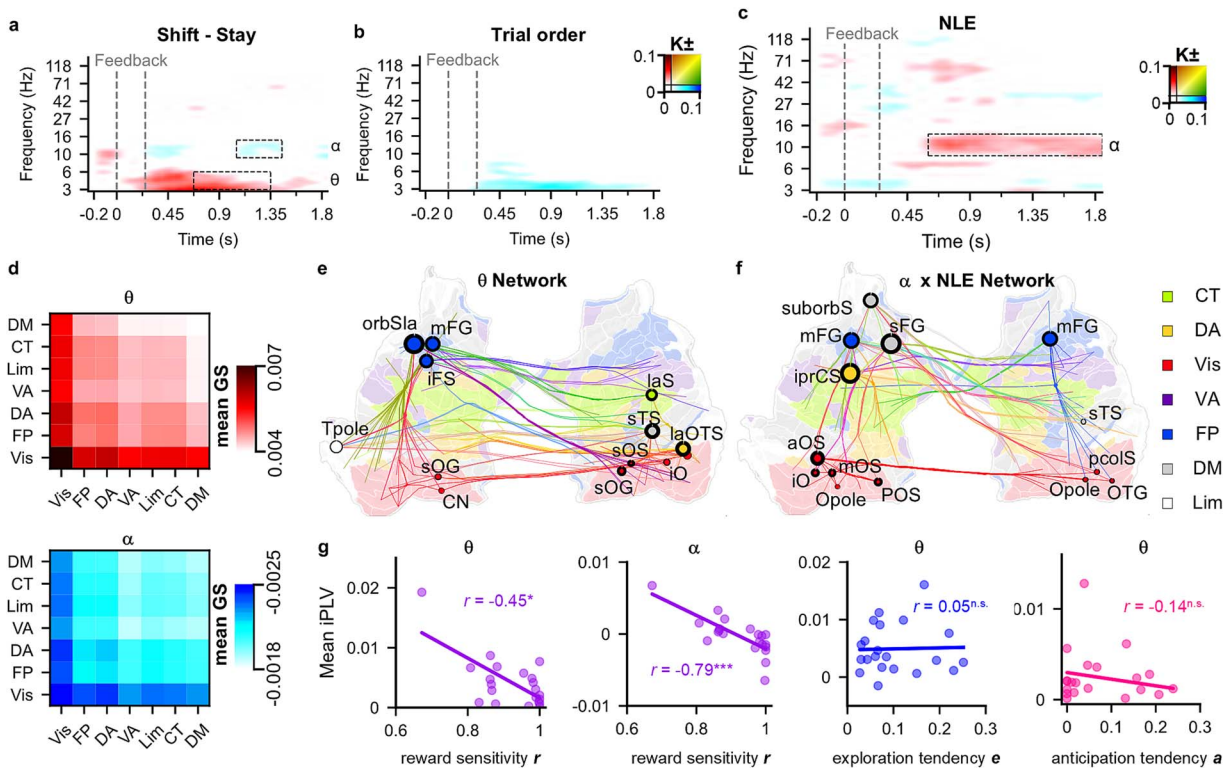

Figure 4 Phase synchrony (iPLV) results for shift and stay conditions, the correlations with performance and the model fit. a. Interareal phase-synchronization for the shift and stay trials compared to the baseline and their contrast shift-stay (Wilcoxon signed-rank test, $P < 0.05$, FDR corrected, q = 0.0067) across participants ($n = 23$). Color indicates the connection density (K) of significant connections. b. Trial series effect showing the fraction of edges whose strength significantly increased or decreased across a rule set (Spearman's r, $P < 0.05$, FDR corrected, q = 0.0067). c. Correlation of the strength of phase synchronization for each edge with NLE by frequency band (Spearman's r, $P < 0.05$, FDR corrected, q = 0.0067). d. Mean graph strength (mean GS) averaged over the functional networks in the θ band (3–6 Hz, top) and α band (9–13 Hz, bottom) in the TF window outlined in panel a. e. θ-band (3–6 Hz, 0.7–1.3 s) matching graph showing the vertices with the highest degree and the 150 edges with the strongest phase-synchronization. Graphs are visualized on a flattened cortex where the color refers to the functional yeo-network. Lines indicate the 200 edges with highest degree and are colored according to the connected parcels and networks. Spheres and annotations indicate nodes, with radii proportional to their degree, and borders proportional to their eigenvector centrality. f. α-band (7–13 Hz, 0.6–1.8 s) matching graph showing the network of the nodes with the largest degrees and strongest edges correlating with NLE. g. Model fit for each subject parameter with the mean edge strength of shift and stay trials ($n = 21$). The color shade expresses the strength of the regression coefficients (Coeff., linear regression, $P < 0.05$, FDR corrected, q = 0.0068). Fitting lines further show the correlation of subjects' mean iPLV values of parcels with a significant model fit and the subject parameters.

Wilcoxon signed-rank test; $P = 0$, r = 0.44) and a small effect size in the α band ($P = 3.34e\text{-}154$, r = 0.18). In order to show that these iPLV effects were not merely reducible to signal to noise ratio changes in oscillation amplitudes, we computed the correlation between θ and α-band amplitudes with the respective iPLV values. iPLV and amplitude values were positively correlated for Shift and Stay trials, but not for their difference (Supp. Fig. 5c), indicating that synchronization is a distinct phenomenon from oscillation amplitudes. The mean strength of phase synchronization correlated across individuals with NLE, such that fewer late errors were predicted by α-band desynchronization (mean r = 0.20) (Fig. 4c). However, the network synchronization did not predict RTs for Shift and only weakly for the Stay condition.

The θ- and α-band synchronization differences between Shift-Stay conditions were driven by functional connections within the visual system and its connections to other networks (Fig. 4d). Visualization of the θ network architecture with the 200 strongest edges and nodes with the largest degrees (i.e. the number of edges with other nodes) revealed major hubs in the PFC (including the middle frontal gyrus (mFG) and inferior frontal sulcus) coupled with nodes of the visual system, such as the superior occipital gyrus and cuneus and lateral occipitotemporal sulcus (Fig. 4e). The visuo-frontal network architecture was thus well supporting the idea of synchronization enabling top-down visual selection of correct rule representation. Similarly, the α-band network related to cognitive flexibility comprised mostly frontoparietal edges between the suborbital sulcus (suborbS), superior and medial frontal gyri (sFG and mFG), inferior precentral sulcus, sTS, anterior occipital sulcus, mid-occipital sulci, iO, the bilateral occipital poles (Opole), parieto-occipital sulcus, pcolS, and the occipitotemporal gyrus (Fig. 4f). To understand how these network effects related to individual differences in feedback processing, we then carried out multivariate regression analysis to identify their correlation with the subject-specific model parameters (Supp. Fig. 6). This showed that α desynchronization was predicted by increased reward sensitivity ***r*** ($P = 0.00002$), but not by other parameters i.e. punishment sensitivity ***p***, anticipation tendency ***a*** or exploration tendency ***e*** (Fig. 4g). θ-band synchronization characteristic to the Shift-Stay difference was also explained by reward sensitivity ($P = 0.04$), and more weakly by anticipation and exploration tendencies, which however were not significantly correlated with θ-band network changes.

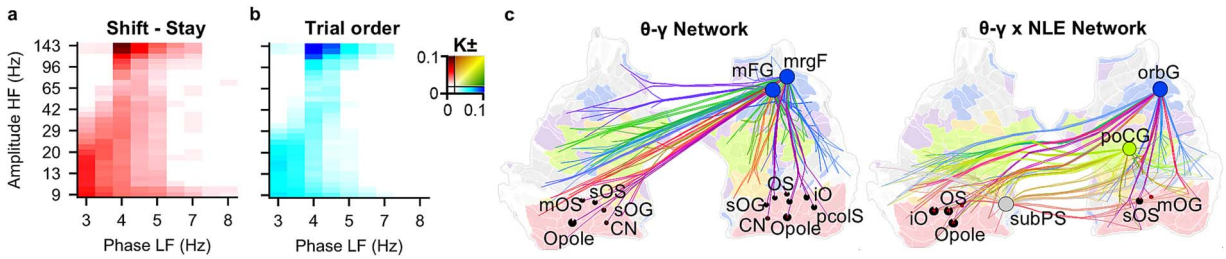

Figure 5 Phase amplitude coupling results for shift and stay conditions, trial order, and the correlations with performance. a. Phase amplitude coupling (PAC) between low-θ frequencies (low frequency, LF) and high-α to γ frequencies (high frequency, HF) during shift and stay trials compared to baseline (surrogate statistics, $P < 0.01$, corrected for spurious connections, q = 0.035) and their contrast (Wilcoxon signed-rank test, $P < 0.05$, FDR corrected, q = 0.00389) across participants ($n = 23$). Color indicates the connection density (K) of significant connections. b. Trial series effect showing the fraction of edges with significant in- or decrease in PAC across a rule set (Spearman's r, $P < 0.05$, FDR corrected, q = 0.00389). c. Positive ($K+$) and negative ($K-$) tails of the correlations of PAC across frequency-band-averaged HFs with NLE, RT_{shift} and RT_{stay} (Spearman's r, $P < 0.05$, q = 0.00281).

Nested coupling of θ phase to α, β, and γ amplitudes predicts task-switching performance

In the previous analysis, we established that local α to γ amplitudes and concurrent θ synchronization are relevant to endogenous task-switching. We then studied if these oscillations could be coupled via PAC. Both Shift and Stay conditions were characterized by strong PAC between θ-band (3–8 Hz) phase and $\alpha - \gamma$ amplitudes (9–143 Hz, Supp. Fig. 7a), of which only the $\theta - \gamma$ PAC was stronger for the Shift than Stay trials (Fig. 5a) and decreased over the course of a rule series (Fig. 5b). Post-hoc analysis revealed that participants with larger PAC showed fewer NLE, RT_{shift} and RT_{stay} (Supp. Fig. 7b). $\theta - \gamma$ PAC was found to connect the θ phase of prefrontal parcels with the γ amplitudes of visual parcels, and the same networks predicted fewer NLE across participants (Fig. 5c).

Discussion

Cognitive flexibility is the ability to quickly adapt behavior to changing environmental demands, such as when making decisions under uncertainty in the absence of instructions and guided only by feedback cues. Behavioral adaptation under these circumstances may require either to keep (Stay with) the current cognitive representation of behavioral rules or to update (Shift) to a new rule. In the real world, this adaptation often depends on the interpretation of ambiguous instructions and environmental cues with high uncertainty. Individuals vary widely in their ability of such cognitive switching between mental representations as well as on their ability to interpret environmental cue information with high uncertainty. The precise neural reasons of these behaviors have remained unknown along with a limited understanding of how feedback processing could influence maintenance and updating between the internal representations of the contextual rules. Using advanced analysis of MEG oscillation dynamics and a new computational modeling approach of behavioral performance, we demonstrate that both local $\alpha - \beta$ as well as γ band oscillations and their large-scale networks predict individual variability in the flexible switching between established and new cognitive representations, each reflecting distinct subprocesses related to feedback processing. While we also found strengthened θ-band oscillation amplitudes and phase synchronization related to task switching, in contrast to previous findings, these did not predict more successful shifting between rules but rather were associated with high task uncertainty.

We show that the subprocesses underlying interindividual variability in cognitive flexibility are explained by differences in positive (reward) and negative (punishment) feedback sensitivity, as well as by exploration tendency, i.e. the tendency to update the cognitive rule representation despite positive feedback. Importantly, this variability was not driven by demographic factors such as sex or age in our sample likely due to the young age of our participants (Rhodes 2004), verifying that interindividual differences in oscillatory modulations can be expected to reflect actual differences in cognitive flexibility.

We further show that oscillation dynamics explain the interindividual variability in cognitive flexibility. Enhanced broad-band γ-band (42–143 Hz) amplitudes and concurrent suppression of $\alpha - \beta$ (13–32 Hz) band amplitudes and synchronization predicted the ability to switch between cognitive representations and the rapidity thereof. The computational modeling of individual performance at the single-trial level established that α- and β-band amplitude suppression predicted more rapid cognitive flexibility as a result of subjects' increased reward sensitivity, while in contrast the behavioral advantage of increased broad-band γ amplitudes arose from higher punishment sensitivity. Thus, $\alpha - \beta$ band amplitude suppression and the increase in broad-band γ amplitudes assigned to different neural sub-processes predicted the variance in cognitive flexibility across individuals.

The importance of $\alpha - \beta$-band amplitudes in updating cognitive representations in the WSCT aligns with previous research that linked α oscillations to switching between brain states favoring visuospatial working memory stability or encoding flexibility (Ericson et al. 2025) and behavioral task switching in sensor-level EEG (Verstraeten and Cluydts 2002; Foxe et al. 2014) and combined EEG-beamforming with an artificial neural network in a recent study (Elmers et al. 2026). Here, we demonstrate that local and large-scale $\alpha - \beta$ oscillations underlie the flexible updating of task rules under uncertainty. We speculate that this association was linked to individual reward sensitivity due to the strong association of α oscillations with engagement vs. disengagement found for visuospatial attention (Bonnefond and Jensen 2025; Eidelman-Rothman et al. 2025) putatively through their modulation of excitability (Iemi et al. 2017; Lange et al. 2013). Reward-related modulation of α oscillations was found in the ventromedial PFC that has earlier been shown to play a major role in reward processing and decision making (Kennerley and Walton 2011; Domenech and Koechlin 2015). Therefore, $\alpha - \beta$ band suppression over the PFC and PPC appear to improve reward-related cognitive flexibility through enhanced reward-driven attentional control.

In addition to local amplitude modulations, fronto-parietal α desynchronization mediated by higher individual reward sensitivity predicted higher individual behavioral cognitive flexibility, albeit with smaller effect sizes. This is in contrast with the association of large-scale increase in $\alpha - \beta$ synchronization with top-down attention (Doesburg et al. 2009; Lobier et al. 2018) and positive correlation with task performance (Palva et al. 2010; Sattelberger et al. 2024). We propose that in the context of the present task, disengagement of the α network serves as a reset of the internal top-down goal, i.e. the current cognitive rule representation. This is supported by some earlier studies in which α desynchronization during visual tasks was related to the tuning of attention in presence of competing sensory stimuli (Gross et al. 2004; Mylonas et al. 2016).

As a distinct neural sub-process of cognitive flexibility, we found a sustained increase in broad-band γ amplitudes that was associated with the processing of negative feedback. In line with γ amplitudes being associated with punishment sensitivity, this modulation was found over the left cingulate cortex, which plays a central role in error monitoring (Carter et al. 1998; Walton et al. 2007). This suggests that broad-band γ (42–143 Hz) amplitudes track the processing of errors and negative feedback in order to enable fast switching of cognitive representations based on contextual demands. However, one should note that the broad-band activity γ cannot be collapsed to a single neuronal phenomenon (Vinck et al. 2023). Instead, transient increases in spiking activity are proposed to mediate feedforward transmission of prediction errors which result in increases in broadband γ power (Canales-Johnson et al. 2021; Uran et al. 2022). This newer account supports our finding of amplified broadband γ amplitudes in Shift trials compared to Stay trials modulated by higher punishment sensitivity to be a signature mechanism of error processing in cognitive flexibility.

In contrast with a large body of EEG research showing that prefrontal and midline θ-band amplitudes enable cognitive flexibility control (Cooper et al. 2015; Duprez et al. 2020; Riddle et al. 2020; Sauseng and Liesefeld 2020; Muralidharan et al. 2023; Khan et al. 2025), here, we found θ amplitudes to strengthen during Shift trials, but not to enhance behavior directly as would be seen in fewer NLEs. In contrast, a decrease in θ amplitudes predicted increased rule certainty across a trial series in our study and were explained by a tendency to anticipate rule changes in line with earlier studies associating prefrontal θ oscillations with task uncertainty (Kosciessa et al. 2021; Kosciessa et al. 2024). Our results thus indicate that increased θ amplitudes are not a facilitating mechanism for switching and updating between cognitive representations per se but rather characterize meta-contextual learning and anticipation of a new rule, and as such, can be associated with more complex preparatory and monitoring processes or contextual updating of information (Cooper et al. 2016). Similarly, stronger prefrontal θ-band network synchronization was not directly linked to performance differences, but to a decreased reward and anticipation tendency, and to increased exploration tendency. Our results therefore provide new evidence that large-scale networks of prefrontal θ-band network synchronization might be a crucial neural inter-areal mechanism for rule exploration and internally guided flexible task-learning. The close correlation of oscillation amplitudes and synchronization values is consistent with the hypothesis that synchronization reflects the consequence of communication and correlation of post-synaptic potentials across areas (Schneider et al. 2021), although synchronization specific modulations between Shift-Stay trials could also be attributed to CTC (Fries 2015; Voloh and Womelsdorf 2016) or CTR frameworks (Hahn et al. 2014; Vinck et al. 2023).

Moreover, PAC of frontal θ amplitudes with broadband γ activity over posterior visual areas tightly associated with feedback processing could reflect phasic control of prefrontal θ oscillations with sensory cortex (Fig. 5c). In particular, the $\theta - \gamma$ PAC between the right dorsolateral PFC and bilateral parietal and visual cortices predicted better behavioral performance with fewer NLE, and shorter RT_{shift} and RT_{stay}, While there is emerging evidence pointing out the significance of nested oscillations and specifically $\theta - \gamma$ coupling for cognitive functioning in attention and working memory (Lisman and Jensen 2013; Brooks et al. 2020; Spooner et al. 2020) and global cognitive control (Turi et al. 2020; Riddle et al. 2021), we prove here also its role in task switching. Such $\theta - \gamma$ PAC could allow for rapid communication between brain areas to implement pro- and reactive phasic cognitive control (Voytek et al. 2015; Verguts 2017; Pagnotta et al. 2024) and coordinate the top-down selection of the correct rule set in the WCST. This interpretation is supported by our finding that $\theta - \gamma$ PAC decreased over the course of a rule series.

Conclusions

Our results demonstrate that the inter-individual variability in cognitive flexibility depends on differential sensitivity to feedback, which maps on to distinct oscillatory sub-processes. Our results therefore provide novel neural signatures for the maintenance and updating of cognitive representations of contextual rules that predict the individual speed of rule learning.

Acknowledgments

The authors would like to thank Jasmin Elonen for preprocessing the MEG data.

Author contributions

Judith Sattelberger (Conceptualization, Data curation, Formal analysis, Investigation, Methodology, Project administration, Software, Visualization, Writing—original draft), Hamed Haque (Conceptualization, Methodology), Liu Mengxing (Formal analysis, Methodology), Jaana Simola (Data curation, Investigation, Software), J Matias Palva (Conceptualization, Funding acquisition, Methodology, Resources, Writing—review & editing), Michael M Halassa (Conceptualization, Methodology, Writing—review & editing), Satu Palva (Conceptualization, Funding acquisition, Methodology, Project administration, Supervision, Visualization, Writing—original draft, Writing—review & editing)

Supplementary material

Supplementary material is available at *CERCOR Journal* online.

Conflicts of interest

The authors declare no competing financial interests.

Funding

This work was supported by the Sigrid-Juselius-Foundation (grant number 240156 to S.P. and J.M.P.).

References

Axmacher N et al. 2010. Cross-frequency coupling supports multi-item working memory in the human hippocampus. *Proceedings of the National Academy of Sciences*. 107:3228–3233.

Bahramisharif A, Jensen O, Jacobs J, Lisman J. 2018. Serial representation of items during working memory maintenance at letter-selective cortical sites. *PLOS Biology*. 16:e2003805.

Baillet S. 2017. Magnetoencephalography for brain electrophysiology and imaging. *Nat Neurosci*. 20:327–339. https://doi.org/10.1038/nn.4504.

Barcelo F. 2003. The Madrid card sorting test (MCST): a task switching paradigm to study executive attention with event-related potentials. *Brain Res Protocol*. 11:27–37. https://doi.org/10.1016/S1385-299X(03)00013-8.

Berg EA. 1948. A simple objective technique for measuring flexibility in thinking. *J Gen Psychol*. 39:15–22. https://doi.org/10.1080/00221309.1948.9918159.

Berger B, Sauseng P. 2022. Brain rhythms: How control gets into working memory. *Curr Biol*. 32:R479–r481. https://doi.org/10.1016/j.cub.2022.04.036.

Biel, AL, Minarik T, Sauseng P. 2021. EEG cross-frequency phase synchronization as an index of memory matching in visual search. *NeuroImage*. 235:117971.

Bishara AJ et al. 2010. Sequential learning models for the Wisconsin card sort task: assessing processes in substance dependent individuals. *J Math Psychol*. 54:5–13. https://doi.org/10.1016/j.jmp.2008.10.002.

Bissonette GB, Powell EM, Roesch MR. 2013. Neural structures underlying set-shifting: roles of medial prefrontal cortex and anterior cingulate cortex. *Behav Brain Res*. 250:91–101. https://doi.org/10.1016/j.bbr.2013.04.037.

Bonnefond M, Jensen O. 2025. The role of alpha oscillations in resisting distraction. *Trends Cogn Sci*. 29:368–379. https://doi.org/10.1016/j.tics.2024.11.004.

Brooks H et al. 2020. Theta-gamma coupling and ordering information: a stable brain-behavior relationship across cognitive tasks and clinical conditions. *Neuropsychopharmacology*. 45:2038–2047. https://doi.org/10.1038/s41386-020-0759-z.

Buckley MJ et al. 2009. Dissociable components of rule-guided behavior depend on distinct medial and prefrontal regions. *Science*. 325:52–58.

Canales-Johnson A et al. 2021. Broadband dynamics rather than frequency-specific rhythms underlie prediction error in the primate auditory cortex. *J Neurosci*. 41:9374–9391. https://doi.org/10.1523/jneurosci.0367-21.2021.

Canales-Johnson A et al. 2023. Feedback information transfer in the human brain reflects bistable perception in the absence of report. *PLoS Biol*. 21:e3002120. https://doi.org/10.1371/journal.pbio.3002120.

Cansler HL et al. 2023. Organization and engagement of a prefrontal-olfactory network during olfactory selective attention. *Cerebral Cortex*. 33:1504–1526.

Carter CS et al. 1998. Anterior cingulate cortex, error detection, and the online monitoring of performance. *Science*. 280:747–749. https://doi.org/10.1126/science.280.5364.747.

Chen K-H et al. 2022. Theta low-gamma phase amplitude coupling in the human orbitofrontal cortex increases during a conflict-processing task. *Journal of Neural Engineering*. 19:016026.

Cohen MX et al. 2009. Good vibrations: cross-frequency coupling in the human nucleus accumbens during reward processing. *Journal of Cognitive Neuroscience*. 21:875–889.

Colom LV, Christie BR, Bland BH. 1988. Cingulate cell discharge patterns related to hippocampal EEG and their modulation by muscarinic and nicotinic agents. *Brain Res*. 460:329–338. https://doi.org/10.1016/0006-8993(88)90377-0.

Cooper PS et al. 2015. Theta frontoparietal connectivity associated with proactive and reactive cognitive control processes. *NeuroImage*. 108:354–363. https://doi.org/10.1016/j.neuroimage.2014.12.028.

Cooper PS, Darriba Á, Karayanidis F, Barceló F. 2016. Contextually sensitive power changes across multiple frequency bands underpin cognitive control. *NeuroImage*. 132:499–511. https://doi.org/10.1016/j.neuroimage.2016.03.010.

Cunillera T et al. 2012. Brain oscillatory activity associated with task switching and feedback processing. *Cogn Affect Behav Neurosci*. 12:16–33. https://doi.org/10.3758/s13415-011-0075-5.

D'Andrea A et al. 2019. Alpha and alpha-beta phase synchronization mediate the recruitment of the visuospatial attention network through the superior longitudinal fasciculus. *NeuroImage*. 188:722–732. https://doi.org/10.1016/j.neuroimage.2018.12.056.

Doesburg SM, Green JJ, McDonald JJ, Ward LM. 2009. From local inhibition to long-range integration: a functional dissociation of alpha-band synchronization across cortical scales in visuospatial attention. *Brain Res*. 1303:97–110. https://doi.org/10.1016/j.brainres.2009.09.069.

Domenech P, Koechlin E. 2015. Executive control and decision-making in the prefrontal cortex. *Curr Opin Behav Sci*. 1:101–106. https://doi.org/10.1016/j.cobeha.2014.10.007.

Domenech P, Rheims S, Koechlin E. 2020. Neural mechanisms resolving exploitation-exploration dilemmas in the medial prefrontal cortex. *Science*. 369:eabb0184. https://doi.org/doi:10.1126/science.abb0184.

Duprez J, Gulbinaite R, Cohen MX. 2020. Midfrontal theta phase coordinates behaviorally relevant brain computations during cognitive control. *NeuroImage*. 207:116340. https://doi.org/10.1016/j.neuroimage.2019.116340.

Eidelman-Rothman M et al. 2025. Quantifying variability in attentional shifts during target switching. *Cereb Cortex*. 35:bhaf329. https://doi.org/10.1093/cercor/bhaf329.

Elmers J, Mückschel M, Ziemssen T, Beste C. 2026. Preparatory alpha-band modulations of directed information transfer in frontoparietal circuits support adaptive behavior. *J Cogn Neurosci*. 38:1450–1471. https://doi.org/10.1162/JOCN.a.2485.

Ericson J, Ruiz Ibáñez N, Lundqvist M, Klingberg T. 2025. Low frequency oscillations - neural correlates of stability and flexibility in cognition. *Nat Commun*. 16:5381. https://doi.org/10.1038/s41467-025-60821-2.

Esghaei M, Treue S, Vidyasagar TR. 2022. Dynamic coupling of oscillatory neural activity and its roles in visual attention. *Trends in Neurosciences*. 45:323–335.

Foxe JJ, Murphy JW, De Sanctis P. 2014. Throwing out the rules: anticipatory alpha-band oscillatory attention mechanisms during task-set reconfigurations. *Eur J Neurosci*. 39:1960–1972. https://doi.org/10.1111/ejn.12577.

Fries P. 2015. Rhythms for Cognition: Communication through Coherence [Review]. *Neuron*. 88:220–235. https://doi.org/10.1016/j.neuron.2015.09.034.

Gamboz N, Erika B, Brandimonte MA. 2009. The role of switching, inhibition and working memory in older adults' performance in the

Wisconsin card sorting test. *Aging Neuropsychol Cognit*. 16:260–284. https://doi.org/10.1080/13825580802573045.
Gladwin TE, Lindsen JP, de Jong R. 2006. Pre-stimulus EEG effects related to response speed, task switching and upcoming response hand. *Biol Psychol*. 72:15–34. https://doi.org/10.1016/j.biopsycho.2005.05.005.
Gross J et al. 2004. Modulation of long-range neural synchrony reflects temporal limitations of visual attention in humans. *Proc Natl Acad Sci*. 101:13050–13055. https://doi.org/doi:10.1073/pnas.0404944101.
Hahn G, Bujan AF, Frégnac Y, Aertsen A, Kumar A. 2014. Communication through Resonance in Spiking Neuronal Networks. *PLoS Computational Biology*. 10:e1003811. https://doi.org/10.1371/journal.pcbi.1003811.
Haque H et al. 2025. Top-down selection of visual working memory contents is supported by alpha-band phase-synchronized oscillatory networks. *Imaging Neuroscience*. 3. https://doi.org/10.1162/imag.a.1034.
Heaton RK, Staff PAR. 1993. Wisconsin card sorting test: computer version 2. *Odessa: Psychological Assessment Resources*. 4:1–4.
Iemi L, Chaumon M, Crouzet SM, Busch NA. 2017. Spontaneous neural oscillations bias perception by modulating baseline excitability. *J Neurosci*. 37:807–819.
JASP Team. 2024. *JASP (version 0.18.3)[computer software]*.
Kennerley SW, Walton ME. 2011. Decision making and reward in frontal cortex: complementary evidence from neurophysiological and neuropsychological studies. *Behav Neurosci*. 125:297–317. https://doi.org/10.1037/a0023575.
Khan AU et al. 2025. Neural dynamics of proactive and reactive cognitive control in medial and lateral prefrontal cortex. *iScience*. 28:113375. https://doi.org/10.1016/j.isci.2025.113375.
Korhonen O, Palva S, Palva JM. 2014. Sparse weightings for collapsing inverse solutions to cortical parcellations optimize M/EEG source reconstruction accuracy. *J Neurosci Methods*. 226:147–160. https://doi.org/10.1016/j.jneumeth.2014.01.031.
Kosciessa JQ, Lindenberger U, Garrett DD. 2021. Thalamocortical excitability modulation guides human perception under uncertainty. *Nat Commun*. 12:2430. https://doi.org/10.1038/s41467-021-22511-7.
Kosciessa JQ, Mayr U, Lindenberger U, Garrett DD. 2024. Broadscale dampening of uncertainty adjustment in the aging brain. *Nat Commun*. 15:10717. https://doi.org/10.1038/s41467-024-55416-2.
Kuwabara M, Mansouri FA, Buckley MJ, Tanaka K. 2014. Cognitive control functions of anterior cingulate cortex in macaque monkeys performing a Wisconsin card sorting test analog. *J Neurosci*. 34:7531–7547.
Lam NH et al. 2025. Prefrontal transthalamic uncertainty processing drives flexible switching. *Nature*. 637:127–136. https://doi.org/10.1038/s41586-024-08180-8.
Lange J, Oostenveld R, Fries P. 2013. Reduced occipital alpha power indexes enhanced excitability rather than improved visual perception. *J Neurosci*. 33:3212–3220.
Lisman JE, Jensen O. 2013. The theta-gamma neural code. *Neuron*. 77:1002–1016. https://doi.org/10.1016/j.neuron.2013.03.007.
Liu Y, Wang X-J. 2024. Flexible gating between subspaces in a neural network model of internally guided task switching. *Nat Commun*. 15:6497.
Lobier M, Palva JM, Palva S. 2018. High-alpha band synchronization across frontal, parietal and visual cortex mediates behavioral and neuronal effects of visuospatial attention. *NeuroImage*. 165:222–237. https://doi.org/10.1016/j.neuroimage.2017.10.044.
Mamashli F et al. 2021. Synchronization patterns reveal neuronal coding of working memory content. *Cell Rep*. 36:109566. https://doi.org/10.1016/j.celrep.2021.109566.
Mansouri FA, Matsumoto K, Tanaka K. 2006. Prefrontal cell activities related to monkeys' success and failure in adapting to rule changes in a Wisconsin card sorting test analog. *J Neurosci*. 26:2745–2756.
Miyake A et al. 2000. The Unity and Diversity of executive functions and their contributions to complex "frontal lobe" tasks: a latent variable analysis. *Cogn Psychol*. 41:49–100. https://doi.org/10.1006/cogp.1999.0734.
Muralidharan V, Aron AR, Cohen MX, Schmidt R. 2023. Two modes of midfrontal theta suggest a role in conflict and error processing. *NeuroImage*. 273:120107. https://doi.org/10.1016/j.neuroimage.2023.120107.
Mylonas D, Siettos C, Evdokimidis I, Papanicolaou A, Smyrnis N. 2016. Modular patterns of phase desynchronization networks during a simple visuomotor task. *Brain Topogr*. 29:118–129.
Nyhus E, Barceló F. 2009. The Wisconsin card sorting test and the cognitive assessment of prefrontal executive functions: a critical update. *Brain Cogn*. 71:437–451. https://doi.org/10.1016/j.bandc.2009.03.005.
Pagnotta MF, Riddle J, D'Esposito M. 2024. Multimodal neuroimaging of hierarchical cognitive control. *Biol Psychol*. 193:108896. https://doi.org/10.1016/j.biopsycho.2024.108896.
Palva JM, Monto S, Kulashekhar S, Palva S. 2010. Neuronal synchrony reveals working memory networks and predicts individual memory capacity. *Proc Natl Acad Sci*. 107:7580. https://doi.org/10.1073/pnas.0913113107.
Palva JM et al. 2018. Ghost interactions in MEG/EEG source space: a note of caution on inter-areal coupling measures. *NeuroImage*. 173:632–643. https://doi.org/10.1016/j.neuroimage.2018.02.032.
Panikratova YR et al. 2020. Functional connectivity of the dorsolateral prefrontal cortex contributes to different components of executive functions. *Int J Psychophysiol*. 151:70–79. https://doi.org/10.1016/j.ijpsycho.2020.02.013.
Papaioannou O et al. 2022. Is cortical theta-gamma phase-amplitude coupling memory-specific? *Brain Sciences*. 12:1131.
Periánez JA et al. 2004. Spatiotemporal brain dynamics during preparatory set shifting: MEG evidence. *NeuroImage*. 21:687–695.
Pesaran B, Nelson MJ, Andersen RA. 2008. Free choice activates a decision circuit between frontal and parietal cortex. *Nature*. 453:406–409. https://doi.org/10.1038/nature06849.
Peylo C, Friedrich EV, Minarik T, Biel AL, Sauseng P. 2022. Theta: gamma phase coupling and evoked gamma activity reflect the fidelity of mental templates during memory matching in visual perception. *Cerebral Cortex*. 32:4156–4171.
Proskovec AL, Wiesman AI, Wilson TW. 2019. The strength of alpha and gamma oscillations predicts behavioral switch costs. *NeuroImage*. 188:274–281. https://doi.org/10.1016/j.neuroimage.2018.12.016.
Puoliväli T, Palva S, Palva JM. 2020. Influence of multiple hypothesis testing on reproducibility in neuroimaging research: a simulation study and python-based software. *J Neurosci Methods*. 337:108654. https://doi.org/10.1016/j.jneumeth.2020.108654.
Ratcliffe O, Shapiro K, Staresina BP. 2022. Fronto-medial theta coordinates posterior maintenance of working memory content. *Curr Biol*. 32:2121–2129.e2123. https://doi.org/10.1016/j.cub.2022.03.045.
Rhodes MG. 2004. Age-related differences in performance on the Wisconsin card sorting test: a meta-analytic review. *Psychol Aging*. 19:482.
Riddle J, McFerren A, Frohlich F. 2021. Causal role of cross-frequency coupling in distinct components of cognitive control. *Prog Neurobiol*. 202:102033. https://doi.org/10.1016/j.pneurobio.2021.102033.
Riddle J, Scimeca JM, Cellier D, Dhanani S, D'Esposito M. 2020. Causal evidence for a role of theta and alpha oscillations in the control of working memory. *Curr Biol*. 30:1748–1754.e1744. https://doi.org/10.1016/j.cub.2020.02.065.

Rikhye RV, Gilra A, Halassa MM. 2018. Thalamic regulation of switching between cortical representations enables cognitive flexibility. *Nat Neurosci*. 21:1753–1763. https://doi.org/10.1038/s41593-018-0269-z.

Robbins TW et al. 1996. Dissociating executive functions of the prefrontal cortex. *Philos Trans R Soc Lond Ser B Biol Sci*. 351:1463–1471. https://doi.org/10.1098/rstb.1996.0131.

Roberts L et al. 2026. Broadband synergy versus oscillatory redundancy in the visual cortex. *Nature Communications*. https://doi.org/10.1038/s41467-026-72444-2.

Rosenthal R. 1991. Effect sizes: Pearson's correlation, its display via the BESD, and alternative indices. *American Psychologist*. 46:1086–1087. https://doi.org/10.1037/0003-066X.46.10.1086.

Rouhinen S, Siebenhühner F, Palva JM, Palva S. 2020. Spectral and anatomical patterns of large-scale synchronization predict human attentional capacity. *Cereb Cortex*. 30:5293–5308.

Sattelberger J et al. 2024. Local and interareal alpha and low-beta band oscillation dynamics underlie the bilateral field advantage in visual working memory. *Cereb Cortex*. 34:bhae448. https://doi.org/10.1093/cercor/bhae448.

Sauseng P, Liesefeld HR. 2020. Cognitive control: brain oscillations coordinate human working memory. *Curr Biol*. 30:R405–R407. https://doi.org/10.1016/j.cub.2020.02.067.

Schneider M et al. 2021. A mechanism for inter-areal coherence through communication based on connectivity and oscillatory power. *Neuron*. 109:4050-4067. https://doi.org/10.1016/j.neuron.2021.09.037.

Siebenhühner F et al. 2020. Genuine cross-frequency coupling networks in human resting-state electrophysiological recordings. *PLoS Biol*. 18:e3000685. https://doi.org/10.1371/journal.pbio.3000685.

Siebenhühner F, Wang SH, Palva JM, Palva S. 2016. Cross-frequency synchronization connects networks of fast and slow oscillations during visual working memory maintenance. *eLife*. 5:e13451. https://doi.org/10.7554/eLife.13451.

Siegel M, Donner TH, Engel AK. 2012. Spectral fingerprints of large-scale neuronal interactions. *Nat Rev Neurosci*. 13:121–134. https://doi.org/10.1038/nrn3137.

Spooner RK, Wiesman AI, Proskovec AL, Heinrichs-Graham E, Wilson TW. 2020. Prefrontal theta modulates sensorimotor gamma networks during the reorienting of attention. *Hum Brain Mapp*. 41:520–529. https://doi.org/10.1002/hbm.24819.

Talk A, Kang E, Gabriel M. 2004. Independent generation of theta rhythm in the hippocampus and posterior cingulate cortex. *Brain Res*. 1015:15–24. https://doi.org/10.1016/j.brainres.2004.04.051.

Taulu S, Kajola M. 2005. Presentation of electromagnetic multichannel data: the signal space separation method. *J Appl Phys*. 97:124905. https://doi.org/10.1063/1.1935742.

Thut G, Miniussi C, Gross J. 2012. The functional importance of rhythmic activity in the brain. *Curr Biol*. 22:R658–R663. https://doi.org/10.1016/j.cub.2012.06.061.

Turi Z et al. 2020. θ-γ cross-frequency transcranial alternating current stimulation over the trough impairs cognitive control. *eneuro*. 7:ENEURO.0126-20.2020. https://doi.org/10.1523/ENEURO.0126-20.2020.

Uran C et al. 2022. Predictive coding of natural images by V1 firing rates and rhythmic synchronization. *Neuron*. 110:2886–2887. https://doi.org/10.1016/j.neuron.2022.07.021.

Verguts T. 2017. Binding by random bursts: a computational model of cognitive control. *J Cogn Neurosci*. 29:1103–1118. https://doi.org/10.1162/jocn_a_01117.

Verstraeten E, Cluydts R. 2002. Attentional switching-related human EEG alpha oscillations. *NeuroReport*. 13:681–684. https://journals.lww.com/neuroreport/fulltext/2002/04160/attentional_switching_related_human_eeg_alpha.29.aspx.

Vinck M et al. 2023. Principles of large-scale neural interactions. *Neuron*. 111:987–1002. https://doi.org/10.1016/j.neuron.2023.03.015.

Voloh B, Womelsdorf T. 2016. A Role of Phase-Resetting in Coordinating Large Scale Neural Networks During Attention and Goal-Directed Behavior [Review]. *Frontiers in Systems Neuroscience*. 10:2016. https://doi.org/10.3389/fnsys.2016.00018.

Voytek B et al. 2015. Oscillatory dynamics coordinating human frontal networks in support of goal maintenance. *Nat Neurosci*. 18:1318–1324.

Voytek B, Knight RT. 2015. Dynamic network communication as a unifying neural basis for cognition, development, aging, and disease. *Biol Psychiatry*. 77:1089–1097. https://doi.org/10.1016/j.biopsych.2015.04.016.

Walton ME, Croxson PL, Behrens TEJ, Kennerley SW, Rushworth MFS. 2007. Adaptive decision making and value in the anterior cingulate cortex. *NeuroImage*. 36:T142–T154. https://doi.org/10.1016/j.neuroimage.2007.03.029.

Wang L, Kakigi R, Hoshiyama M. 2001. Neural activities during Wisconsin card sorting test — MEG observation. *Cogn Brain Res*. 12:19–31. https://doi.org/10.1016/S0926-6410(01)00022-2.

Wang C, Ulbert I, Schomer DL, Marinkovic K, Halgren E. 2005. Responses of human anterior cingulate cortex microdomains to error detection, conflict monitoring, stimulus-response mapping, familiarity, and orienting. *Journal of Neuroscience*. 25:604–613. https://doi.org/10.1523/jneurosci.4151-04.2005.

Wang SH et al. 2018. Hyperedge bundling: a practical solution to spurious interactions in MEG/EEG source connectivity analyses. *NeuroImage*. 173:610–622.

Womelsdorf T, Johnston K, Vinck M, Everling S. 2010. Theta-activity in anterior cingulate cortex predicts task rules and their adjustments following errors. *Proceedings of the National Academy of Sciences of the United States of America*. 107:5248–5253. https://doi.org/10.1073/pnas.0906194107.

Yang Q, Walker E, Cotton RJ, Tolias AS, Pitkow X. 2021. Revealing nonlinear neural decoding by analyzing choices. *Nature Communications*. 12:6557. https://doi.org/10.1038/s41467-021-26793-9.

Zhang X, Mukherjee A, Halassa MM, Chen ZS. 2025. Mediodorsal thalamus regulates task uncertainty to enable cognitive flexibility. *Nat Commun*. 16:2640. https://doi.org/10.1038/s41467-025-58011-1.

Cerebral Cortex, 2026, **36**, bhag101
https://doi.org/10.1093/cercor/bhag101
Original Article